Ceramics International 52 (2026) 14883–14898

Contents lists available at ScienceDirect

Ceramics International

journal homepage: www.elsevier.com/locate/ceramint

Plasma-assisted polishing with self-limiting surface modification for sub-nanometer finishing of AlN ceramics

Tong Tao, Rongyan Sun *, Yuji Ohkubo, Kazuya Yamamura **

Research Center for Precision Engineering, Graduate School of Engineering, The University of Osaka, 2-1 Yamadaoka, Suita, Osaka, 565-0871, Japan

ARTICLE INFO

Keywords:
Self-limiting surface modification
Ultra-low polishing pressure
Advanced ceramics
Grain-boundary step free

ABSTRACT

Advanced ceramics, typically fabricated by sintering single-crystal grains with a binder phase, retain the intrinsic properties of the raw materials while offering low manufacturing cost and high design flexibility in shape and size, making it widely applicable across diverse fields. To fully exploit its potential, sub-nanometer-level smooth surfaces are required. However, intrinsic inhomogeneities among grains and between grains and the binder phase lead to anisotropic material removal and grain shed-off during conventional mechanical processing, becoming a critical bottleneck to sub-nanometer-level finishing. In this study, the effects of abrasive size and lapping pressure in conventional mechanical lapping were first investigated. Using small-size abrasives at lower pressure effectively suppressed grain shed-off and reduced surface roughness. However, the attainable smoothness was ultimately limited by material inhomogeneity and the threshold pressure required for material removal. To overcome this limitation, plasma-assisted polishing (PAP) that combines self-limiting surface modification with selective removal at ultra-low polishing pressure was developed. Firstly, an easily removable modified layer was formed on the AlN ceramic surface via plasma irradiation. By leveraging the self-limiting reaction characteristics of the modified layer, uniform modification insensitive to grain orientation and phase composition was achieved by controlling modification parameters. Subsequently, this uniform modified layer was selectively removed at a polishing pressure significantly below the conventional removal threshold. Using this approach, a grain-boundary step free and ultra-smooth surface with an average surface roughness *Sa* of 0.86 nm over an 84 μm × 84 μm region was obtained on AlN ceramics. These results demonstrate the feasibility of PAP for achieving sub-nanometer-level finishing of hard-to-machine ceramics represented by AlN, which provides a new processing route for high-power and high-frequency electronic packaging substrates.

1. Introduction

Advanced ceramics can retain the intrinsic merits of raw single-crystal materials while offering low manufacturing cost and high design flexibility in shape and size and have therefore been widely employed in integrated circuits, high-power semiconductor devices, communication electronics, LED components, and precision molds [1,2]. As typical representatives of advanced ceramics, reaction-sintered silicon carbide (RS-SiC) has attracted attention in optical molds, aerospace telescope mirrors, and precision mechanical components due to its high hardness, high thermal conductivity, and low thermal expansion coefficient. Aluminum oxide (Al_2O_3), known for its chemical stability and relatively high hardness, is widely used in cutting tools, sealing components, and wear-resistant parts. Aluminum nitride (AlN) ceramics exhibit a thermal conductivity (theoretical value of ~320 W/m·K) [3,4] far exceeding that of Al_2O_3 [5], which enables efficient heat dissipation in high-power devices [6,7]. Moreover, the thermal expansion coefficient of AlN closely matches those of mainstream semiconductor materials such as Si and GaAs, significantly reducing interfacial stress during thermal cycling and thus preventing joint failure or package cracking. In addition, AlN combines high electrical resistivity, superior mechanical strength, and excellent chemical inertness, making it widely regarded as an ideal substrate material for electronic packaging [8]. With the rapid development of electronics, aerospace, optoelectronic devices, and new energy technologies, the demand for ultra-smooth surfaces in advanced ceramic components and molds has steadily increased to the sub-nanometer level. For RS-SiC, whether as optical elements or as molds, surface roughness directly affects diffuse

* Corresponding author.
** Corresponding author.
E-mail addresses: r-sun@prec.eng.osaka-u.ac.jp (R. Sun), yamamura@prec.eng.osaka-u.ac.jp (K. Yamamura).

https://doi.org/10.1016/j.ceramint.2026.02.123
Received 22 November 2025; Received in revised form 23 January 2026; Accepted 8 February 2026
Available online 10 February 2026

reflectance and thus the imaging quality of optical systems. In the case of AlN substrates for semiconductor device packaging, rough surfaces can generate microscopic voids at the interface of chip and substrate, reducing the actual contact area and heat dissipation [9], which makes it challenging to meet the stringent surface quality requirements of high-power semiconductor device packaging. Therefore, achieving sub-nanometer-level smooth surfaces has become a critical bottleneck for the further application and performance optimization of advanced ceramics.

However, advanced ceramic materials are typically fabricated by sintering single-crystal grains with a binder phase, which not only preserves the inherently difficult-to-machine properties of the crystals such as high hardness, brittleness and chemical inertness, but also introduces significant microstructural inhomogeneity. Variations in grain orientation lead to anisotropic material removal rates, while relatively weak grain boundaries are prone to grain shed-off. Differences between the binder phase (e.g., Y_2O_3 in AlN ceramics) and the crystal grains in hardness, elastic modulus, and chemical reactivity further exacerbate non-uniform removal and step formation. Compared with single-crystal materials, polycrystalline and multiphase ceramics thus present greater challenges in achieving ultra-smooth and damage-free surfaces. To obtain high-quality surfaces on advanced ceramics, various strategies have been explored. For instance, in the case of AlN, Han *et al.* demonstrated that using resin-bonded diamond abrasives with a diameter of 1 μm offers superior processing performance compared with conventional rigid pellet finishing and obtained sub-50 nm surface roughness [10]. However, conventional mechanical finishing is inherently constrained by the threshold pressure required for material removal, as well as the trade-off between efficiency and achievable surface quality. Although applying high polishing pressure or using coarse abrasives can increase the material removal rate (MRR), such conditions easily induce surface and subsurface damage, as well as grain shed-off, leading to step morphology. Conversely, using small size abrasives and low polishing pressure to achieve low surface roughness inevitably results in a drastic decrease in removal rate, making it difficult to meet manufacturing demands. To improve processing efficiency, Katahira *et al.* employed Electrolytic In-Process Dressing (ELID) grinding for AlN ceramics and demonstrated that a #30,000 diamond wheel can produce a mirror surface with *R*a of 8 nm, although further improvement still remains challenging [11]. To mitigate the subsurface damage that is inevitably introduced by conventional mechanical material removal, Zhou *et al.* combined Al_2O_3 abrasive pre-grinding with SiO_2--slurry chemical mechanical polishing (CMP) and achieved a smooth surface with roughness of *R*a 6 nm [12]. Although CMP avoids mechanically induced damage, the chemical components in the slurry increase environmental burden [13]. In addition, AlN is prone to hydrolysis in aqueous environments, which can deteriorate surface roughness, further limiting the applicability of conventional wet polishing processes [14]. To address this issue, a dry polishing process named plasma-assisted polishing (PAP) was proposed, which combines surface modification by plasma irradiation and removal of modified layer. When PAP was applied to AlN ceramics, a surface roughness of *S*a ≈3 nm was obtained, and with a material removal rate approximately twice that of polishing without plasma irradiation [15]. Although the above processes can effectively improve the material removal rate and reduce the surface roughness to several nanometers, differences in chemical reactivity among crystal orientations and material compositions in AlN ceramics inevitably lead to non-uniform surface modification. After removal of the modified layer, grain-boundary step structures remain on the surface, making it challenging to achieve sub-nanometer-level smooth surface. Therefore, achieving uniform modification across different phases and grain orientations is crucial for obtaining sub-nanometer-level smooth surfaces on AlN ceramics.

In classical thermal oxidation, the reaction follows the Deal–Grove model, in which the oxidation rate decreases with increasing oxide thickness and finally approaches saturation, exhibiting a typical self-limiting behavior. This process is mainly governed by diffusion and is independent of the chemical activities of the material. However, the thermal oxidation rate are inherently slow and inefficient for practical processing. Similar to thermal oxidation, plasma modification is also driven by chemical reactions between highly reactive radicals and the substrate surface. As the modified layer grows, the radicals must penetrate the already formed layer and continue to react at the interface, so that the reaction rate gradually become diffusion-limited and eventually reach a saturated modified-layer thickness. This saturated thickness is primarily determined by the penetration depth of the radicals, enabling the formation of a uniform modified layer even on inhomogeneous surfaces. Unlike conventional chemical-modification-assisted polishing, in which the modified layer is removed at an early stage of its formation and thus remains non-uniform on inhomogeneous materials, this study exploits the self-limiting nature of plasma modification. By precisely controlling the modification conditions and plasma irradiation time, a uniform modified layer is first formed on the AlN ceramic surface and subsequently selectively removed, thereby effectively suppressing the influence of material inhomogeneities on the modification rate and enabling a further significant reduction in surface roughness. However, achieving self-limiting modification requires longer plasma irradiation time, which limits the processing efficiency. To reduce the saturation time and improve the efficiency of PAP, the plasma excitation mode was changed from capacitively coupled plasma (CCP) in conventional PAP to inductively coupled plasma (ICP), which provides a much higher radical density. Since the polishing process should be carried out after formation of uniform modified layer, a two-step PAP that combines self-limiting surface modification with selective modified layer removal under ultra-low polishing pressure was proposed. First, CF_4 reaction system is employed to rapidly modify the AlN surface until modification self-limited. This treatment ensures that different grain orientations and phases, including AlN grains and the Y_2O_3 binder phase, achieve a uniform, easily removable modified state. Subsequently, the modified layer is selectively removed using a vitrified bonded diamond grinding stone with small size abrasives and under the polishing pressures well below the conventional mechanical removal threshold, thereby effectively avoiding the introduction of damage to the underlying material. This two-step PAP process is designed to simultaneously suppress brittle material removal and subsurface damage, while avoiding surface steps and roughness deterioration caused by phases and grain orientations differences. It thus provides an efficient, environmentally friendly, and controllable approach for realization of sub-nanometer-level smooth surface preparation of hard-to-machine advanced ceramics.

2. Experimental setup

In this study, AlN ceramic substrate (ϕ 50 mm × 1 mm^t, provided by CoorsTek, Inc.) after grinding was used. First, conventional lapping was conducted to investigate the machining characteristics of AlN ceramics under purely mechanical processing and to identify the limitations of conventional mechanical processes. Subsequently, a two-step PAP process was developed and evaluated, in which self-limiting plasma-induced surface modification was combined with selective removal using small size abrasives under ultra-low polishing pressure. This approach was designed to overcome the limitations of conventional mechanical polishing in terms of surface quality and efficiency and to achieve sub-nanometer-level polishing of AlN ceramics.

Fig. 1 illustrates a schematic of the lapping equipment (EJ-380IN-D, ENGIS) used in this study. As a commonly employed planarization technique, lapping is generally classified into two types based on the type of abrasive state, free-abrasive lapping and fixed-abrasive lapping. In free-abrasive lapping, a soft metal plate serves as the reference surface, and material removal and surface planarization are achieved using a slurry containing free abrasives [16]. However, free-abrasive lapping suffers from low material removal efficiency and issues such as abrasive agglomeration, which can cause peripheral scratches and edge sagging

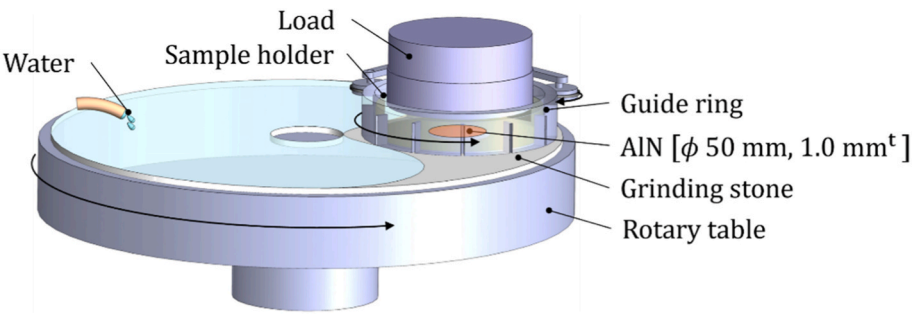

Fig. 1. Schematic of lapping equipment.

on the substrate. To achieve higher planarity and lower surface roughness, fixed-abrasive lapping was employed in this study. A fixed-abrasive polishing plate (provided by MIZUHO Co., Ltd.) was used to replace the conventional soft metal plate and slurry-based free abrasives. Since the abrasives are firmly bonded and the number of abrasives per unit area is significantly increased without agglomeration, a higher MRR can be achieved at the same particle size. Meanwhile, since the abrasives are uniformly distributed and the lapping plate surface can be dressed to correct its reference shape, edge sagging can be suppressed and the planarity of the substrate can be improved. During the lapping process, the AlN substrate was fixed on the sample holder, which was placed inside a guide ring. The drive shaft rotated the guide ring and substrate simultaneously, while the fixed abrasive lapping plate rotated in sync to generate controlled relative motion, enabling material removal and surface planarization of the AlN ceramic.

Fig. 2 shows a schematic of the laboratory-built PAP equipment used in this study. To investigate the mechanisms and characteristics of self-limiting plasma modification and the uniform removal of the modified layer cross grains and phases, a two-step PAP system consisting of an inductively coupled plasma (ICP) modification unit and a fixed-abrasive polishing unit was employed. During the modification stage, the process gases (CF_4 or O_2) were supplied from high-pressure cylinders, and the gas flow rates were precisely controlled via mass flow controllers (MFCs) before being introduced into the vacuum chamber through the bottom of an Al_2O_3 plasma discharge tube (ϕ 60 mm). The chamber pressure was regulated by the combined control of gas flow and the pumping rate of a dry vacuum pump, and stabilized at 37 Pa. An RF power supply (f = 13.56 MHz) was connected to an induction coil wound around the exterior of the Al_2O_3 tube. The RF current induces an alternating magnetic field and a corresponding electric field inside the tube, accelerating electron collisions to generate a high-density plasma. By adjusting the impedance matcher, a stable and uniform discharge can be maintained between the plasma tube and the substrate surface, enabling effective surface modification of the whole AlN substrates. The AlN substrate was fixed at the bottom of a sample holder and placed on an adjustable stage directly above the outlet of the ICP discharge tube. The stage height was precisely controlled to adjust the gap between the substrate and the plasma discharge tube, thereby regulating the uniformity and rate of surface modification. Upon completion of the modification step, the substrate is transferred via an automated carrier arm to the polishing position and positioned inside a guide ring on the polishing plate. The drive shaft rotated the guide ring and substrate simultaneously, while the polishing plate rotated in sync to generate controlled relative motion, selectively removing the modified layer. After polishing, the substrate was returned via the carrier arm to the ICP modification position for the next modification cycle. Through the iterative two-step PAP process of plasma modification and selective removal, ultra-precision surface finishing of AlN ceramics was achieved.

3. Results and discussion

3.1. Mechanical lapping mechanism of AlN ceramics

As a pre-polishing process, conventional mechanical lapping experiments were first conducted on grinding processed AlN ceramic substrates to systematically investigate the effects of abrasive size and nominal lapping pressure on processing characteristics, and to elucidate the material removal mechanisms of AlN ceramic during mechanical processing. The experimental conditions are summarized in Table 1. Initially, a vitrified bonded diamond grinding stone with #6000 coarse abrasives (average diameter 2–3 μm) was used to perform lapping experiments for 1, 2, and 10 min under three different nominal lapping

Table 1
The experimental parameters of lapping process.

Parameters	Conditions
Substrates	AlN ceramic
Lapping pressure	57 kPa/35 kPa/7 kPa (#6000: ϕ 2~3 μm) 57 kPa (#40000: ϕ 0.125 μm)
Type of abrasive	Vitrified-bonded diamond
Lapping plate rotation	60 rpm
Substrate rotation	30 rpm
Water flow rate	5 ml/min

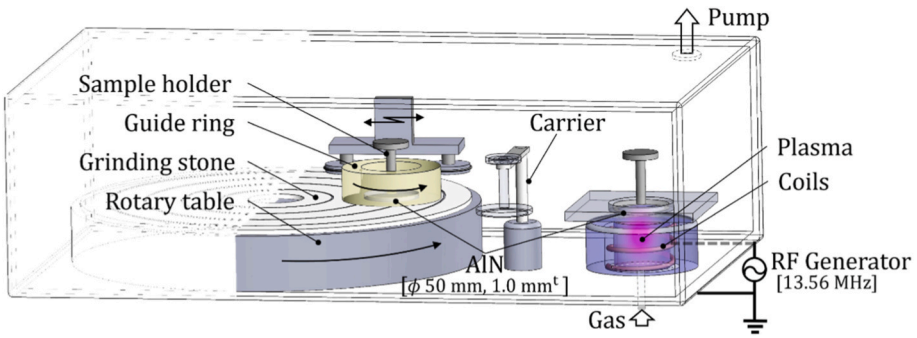

Fig. 2. Schematic of plasma-assisted polishing equipment.

pressures of 57, 35, and 7 kPa respectively. After lapping, the arithmetic mean surface roughness *Sa* was measured at the center and four peripheral points over an 84 μm × 84 μm region using a scanning white-light interferometer (SWLI, NewView 8300, Zygo). The thickness of the substrate at the same five locations before and after lapping was measured using a contact height gauge (DIGIMICRO MFC-101A, Nikon) to calculate the average MRR. The results are shown in Fig. 3 and indicate that lapping pressure has a significant effect on both MRR and surface roughness. Under a nominal lapping pressure of 57 kPa, the surface roughness *Sa* decreased from 612.4 nm to 265.6 nm within 1 min, while the MRR reached a high value of 354 μm/h. When the pressure was reduced to 35 kPa and 7 kPa, the surface roughness further decreased to 223.2 nm and 172.0 nm, respectively, while the MRR dropped to 130.2 μm/h and 19 μm/h. These results are consistent with the Preston equation (MRR = $k{\cdot}P{\cdot}v$, where k is the Preston coefficient, P is the applied pressure, and v is the relative velocity), confirming that the MRR decreases proportionally with decreasing pressure. Moreover, this indicated an inherent trade-off in conventional mechanical processing: improvements in surface roughness come at the cost of a substantial reduction in MRR.

To evaluate the planarization capability at different morphological scales, surface profiles of AlN substrate after grinding and lapping were analyzed (Fig. 4). After 13 min of fixed-abrasive lapping, no edge sagging was observed due to the uniform distribution of abrasives and predressing of the lapping plate. The overall peak-to-valley (PV) value decreased markedly from 9 μm to 0.7 μm, demonstrating that fixed-abrasive lapping can effectively achieve global planarization and decrease the surface roughness. However, during lapping with coarse (#6000) abrasives, the relatively low number of abrasive particles per unit area led to higher local contact pressure and deeper indentation of each abrasive under the same nominal lapping pressure. On the multi-phase and brittle AlN ceramic substrate, this condition more readily led to the AlN grains shed-off, making it difficult to achieve a smooth surface. To reduce the local contact pressure, a vitrified bonded diamond grinding stone with #40000 small-sized abrasives (average diameter 0.125 μm) was introduced for comparison. Marked point observations at the same regions were performed using SWLI and SEM (JSM-IT210LV, JEOL). The results are shown in Fig. 5. When a #6000 grinding stone was used at a lapping pressure of 7 kPa for 10 min with material removal of 3.3 μm, numerous pits appeared on the surface due to the shed-off of AlN grains. By contrast, using a #40000 grinding stone with much smaller abrasives increased the actual contact area between the AlN

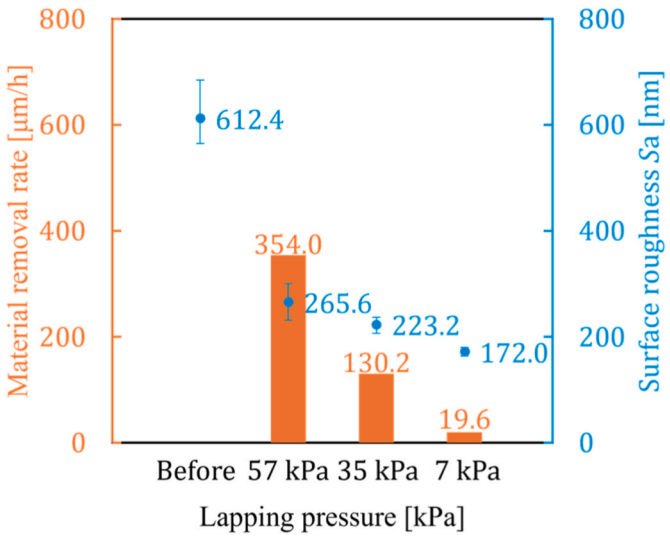

Fig. 3. Comparison of material removal rate and surface roughness *Sa* of AlN ceramic before lapping and after lapping under different lapping pressures using #6000 fixed diamond lapping plate.

substrate and the abrasives, thereby significantly reducing the local contact pressure during lapping. Under this condition, the material removal mechanism shifted from bulk grain shed-off to top-down removal of individual grains. It is noteworthy that the characteristic particle size of the #40000 abrasives is approximately 1/40 of the AlN grain size. At this abrasive-to-grain size ratio, the contact area of individual abrasive was relatively small and tangential forces were more evenly distributed. Even under a higher nominal lapping pressure of 57 kPa, the dominant removal mechanism remained a top-down ductile or quasi-ductile cutting, with virtually no bulk grain shed-off (The black dashed-line region in the SWLI image and The yellow dashed-line region in the SEM image). Correspondingly, the surface roughness *Sa* decreased from 181.9 nm to 46.1 nm within 10 min and continued to decrease with extended lapping time. After 4 h of lapping, the surface roughness *Sa* reached 2.8 nm and no further roughness reduction was observed even when polishing time was further extended, representing the limiting roughness under this lapping pressure. Based on the changes in marked scratch depths, the average MRR was determined to be 1.2 μm/h.

To further reduce the roughness of the AlN surface, the lapping characteristics of the #40000 grinding stone were also evaluated at lower lapping pressures. The results are shown in Fig. 6. At the same observation regions, as the lapping pressure decreased from 57 kPa to 7 kPa, the peak-to-valley height *Sz* decreased from 585 nm to 55 nm, while the corresponding *Sa* decreased from 2.8 nm to 2.4 nm. To achieve even lower lapping pressure and enable direct comparison with subsequent PAP experiments, the substrate was mounted on a lighter PAP sample holder and lapping experiments were performed on the PAP equipment using the same #40000 diamond grinding stone. When the pressure was further reduced to 2 kPa, some pits were removed and *Sa* slightly decreased to 2.1 nm. However, the MRR was only 19.6 nm/h, *Sz* remained nearly unchanged and a considerable number of surface pits still remained. Upon further reducing the pressure to 0.9 kPa, SWLI image showed negligible changes in both surface morphology and roughness. Under this condition, effective brittle or ductile removal of AlN could no longer be achieved. The abrasives merely slid over the surface, causing no damage and failing to further reduce surface roughness.

To investigate the origin of surface pits and the reason why the surface roughness *Sa* and *Sz* could not be further reduced, correlative characterization was performed at the same surface region using AFM (OLS4500, Olympus), SEM, and EDX (JSM-IT210LV, JEOL). As shown in Fig. 7, the surface pits primarily corresponded to bright regions in the SEM images. EDX elemental analysis indicated a significantly absent of Al and N signals in these regions, accompanied by enrichment of Y and O. Based on the composition of the raw materials, these pit regions were identified as the Y_2O_3 binder phase. Because the hardness of Y_2O_3 phase (4.05 GPa) is significantly softer than that of AlN (12.68 GPa) [17,18], it is more readily removed during diamond lapping, resulting in surface pits. Moreover, the relatively weak bonding between Y_2O_3 and AlN can easily cause bulk shed-off of the Y_2O_3 phase [19,20]. In addition, AFM images revealed step from grains and numerous scratches on the AlN surface following purely mechanical removal, which further hindered the reduction of surface roughness.

From the above results, it can be concluded that reducing the abrasive particle size and lowering the nominal lapping pressure can alter the material removal mode of AlN, shifting from bulk grain shed-off to top-down ductile-like removal, thereby effectively decreasing surface roughness. However, due to the inherent differences in grain orientations and phase properties within AlN ceramics, pits and step features remain difficult to completely avoid. In addition, a threshold pressure for material removal exists when the applied pressure falls below this threshold, the abrasives cannot effectively penetrate the surface and merely slide over it, leading to stagnation of material removal.

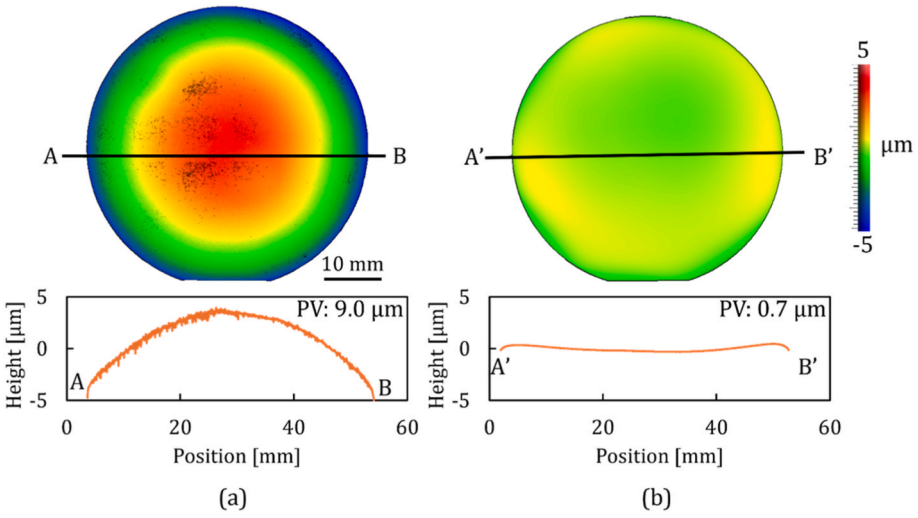

Fig. 4. Flatness of AlN ceramic (a) before lapping and (b) after lapping using #6000 fixed diamond lapping plate.

3.2. CF_4 plasma modification of AlN ceramics

In PAP, only the modified layer can be selectively removed, therefore, both the modification rate and quality of the modified layer are critical factors in the overall PAP process. To balance the modification rate with electrode longevity and to prevent degradation caused by direct contact between the electrode surface and reactive plasma, a non-electrode-based ICP was employed as the plasma source, as described in Section 2. The specific parameters for the plasma modification experiments are listed in Table 2. Before plasma modification, the substrates were cleaned with SPM (H_2SO_4:H_2O_2 = 4:1) and HF solutions to remove surface contaminants. The chemical composition of the AlN surface before and after plasma irradiation was characterized by X-ray photoelectron spectroscopy (XPS) using a Quantum 2000 instrument (ULVAC-PHI) with Al-Kα radiation (1486.6 eV) at a take-off angle of 45°. All spectra were charge-corrected using the C–C peak in C1s spectrum at a binding energy (BE) of 284.8 eV [21]. As shown in Fig. 8(a), the full scan spectrum of AlN surface before plasma irradiation exhibited peaks of Al, N, O. It should be noted that the surface coverage of Y_2O_3 particles is relatively low. Therefore, no characteristic Y peaks were detected in the full scan spectrum. The peak in the Al2p spectrum (Fig. 8(b)) correspond to Al–N (BE = 73.7 eV) and naturally oxidized Al–O (BE = 74.6 eV) [22–24], indicating the presence of a thin naturally formed Al_2O_3 layer. Fig. 8(d) and (e) present the XPS spectra after pure CF_4 plasma irradiation for 30 s, showing no distinct peaks were detected in the Al2p spectrum. While in the C1s spectrum, in addition to the original C–C peak, signals corresponding to C–CF_x, C–F, and C–F_2 were observed (C–C at 284.8 eV, C–CF_x at 286.7 eV, C–F at 288.7 eV, C–F_2 at 290.7 eV) [25]. The full scan spectrum in Fig. 8 (a) also shows the absence of Al, N, and with increasing of C, F. These results indicated that a fluorocarbon deposition layer was formed on the AlN surface, with a thickness exceeding the XPS detection depth and thus preventing the detection of AlN-related peaks. It can be inferred that this deposition layer also blocked the contact between plasma radicals and the AlN surface, severely suppressing the intended modification of AlN. To elucidate the origin of the fluorocarbon deposition, optical emission spectroscopy (OES) measurements of the plasma were conducted. As shown in Fig. 9 (b), in addition to the F emission peak (739.9 nm), strong C_2 Swan band peaks were detected [26], which are considered the primary cause of the fluorocarbon deposition layer and the consequent inhibition of AlN surface modification [27–29]. Based on this, O_2 was introduced into the pure CF_4 plasma to oxidize C_2. With the total gas flow maintained at 100 sccm, the O_2/CF_4 ratios were adjusted and the emission intensities of C_2, F, and O peaks were monitored for each component. As shown in Fig. 9 (c), with increasing O_2 fraction, the O emission intensity increased, while the C_2 intensity decreased as expected due to oxidation. The addition of an appropriate amount of O_2 to the CF_4 plasma effectively promotes CF_4 dissociation [30]. However, excessive O_2 led to competition with CF_4 dissociation, resulting in the F emission intensity initially increasing and then decreasing. The purpose of O_2 addition was to eliminate fluorocarbon deposition on the AlN surface during the modification process, and thus the disappearance of the C_2 peak was considered an indicator of suppressed the deposition. AlN substrates were subjected to plasma modification for 30 s under different O_2/CF_4 ratios, and the surface compositions were analyzed by XPS after treatment. Under the O_2/CF_4 ratio of 91 sccm/9 sccm, the XPS spectra of the modified AlN surface are shown in Fig. 9(a), (d) and (e). The full scan spectrum shows the exhibited peaks of Al, N, F, C and O. No C-F related peaks were detected in the C1s spectrum, indicating that fluorocarbon deposition was fully suppressed. In the Al2p spectrum, in addition to the initial Al-N and Al-O peaks, a new Al-F peak (BE = 75.7 eV) appeared [31]. Based on these results, it can be concluded that under this plasma condition, fluorocarbon deposition which hindered AlN surface modification was effectively suppressed, and the AlN surface was successfully modified to an AlF_3 modified layer.

To establish the relationship between modification time and modified layer thickness, additional plasma irradiation experiments for 1 min and 10 min were performed, and the surface composition was measured by XPS after each irradiation. After 1 min of plasma irradiation, as shown in Fig. 10, the proportion of the Al–F peak in the Al2p spectrum increased significantly compared with that after 30 s, indicating continued growth of the modified layer between 30 s and 1 min. Besides, the absence of Al–N signals in both the Al2p and N1s spectra suggesting that the surface within the XPS detection depth was fully modified. For Al-Kα excitation (1486.6 eV), the approximate kinetic energy of Al2p photoelectrons is 1413(±2) eV. The inelastic mean free paths (IMFPs) for AlF_3 (λ_1) and Al_2O_3 (λ_2) were calculated using the TPP-2M universal formula [32], resulting in IMFP values of approximately 4.09 nm and 3.10 nm, respectively. The thickness of the surface modified layer based on the Beer-Lambert X-ray photoemission decay equation was calculated to exceed 7.2 nm [33]. Since the thickness of modified layer exceeded the XPS detectable depth, the XPS spectra after 10 min of plasma irradiation were found to be identical to those after 1 min.

3.3. Plasma self-limiting modification

In section 3.2, it was demonstrated that CF_4 plasma can efficiently modify the AlN surface within a short time, providing a strong

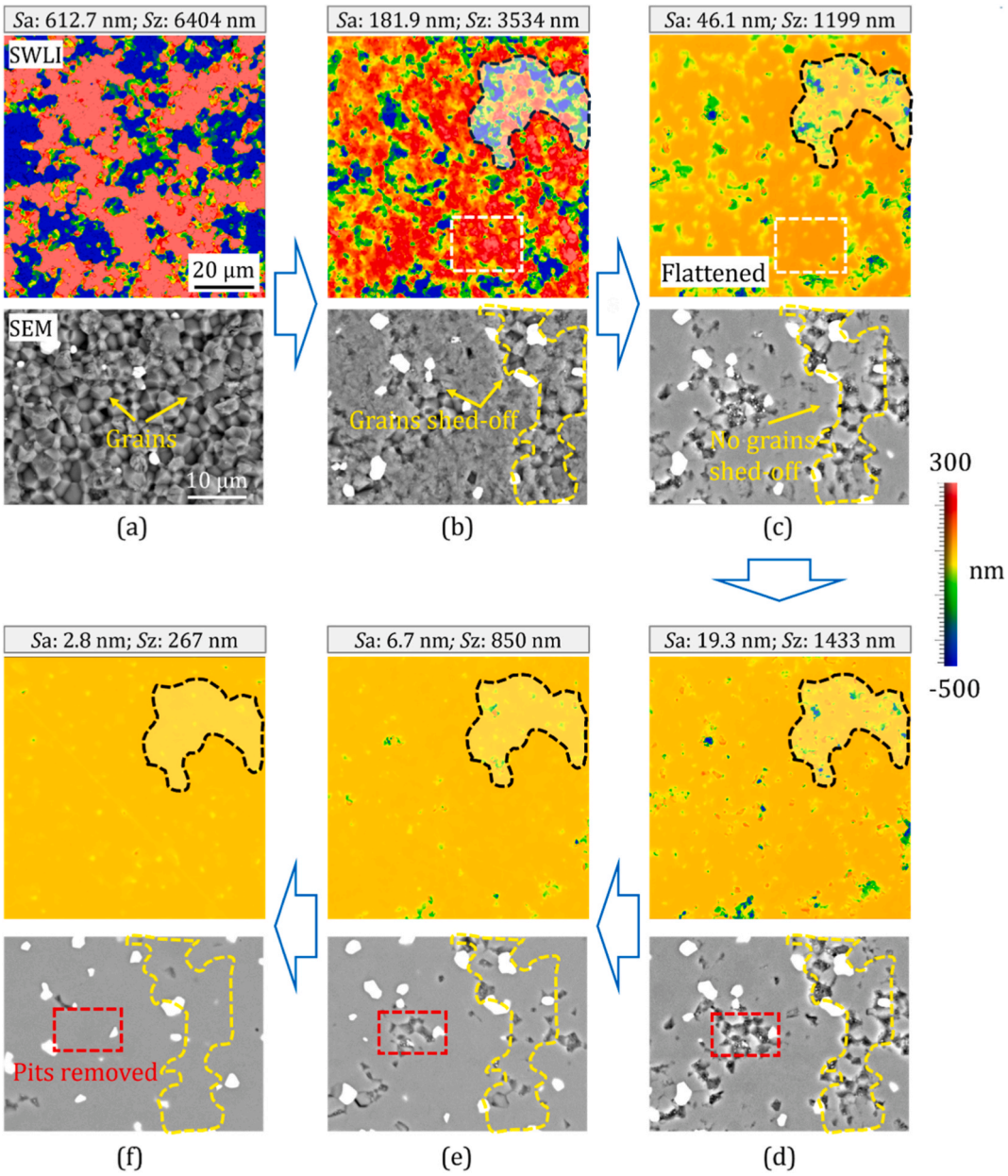

Fig. 5. SWLI and SEM images of the AlN ceramic surface: (a) as-received; (b) after lapping with #6000 diamond abrasive under 7 kPa for 10 min; after lapping with #40000 diamond abrasive under 57 kPa for (c) 10 min, (d) 20 min, (e) 2 h, and (f) 4 h.

foundation for the subsequent selective removal of the modified layer in the PAP process. However, the polycrystalline and multiphase nature of AlN ceramics, consisting of AlN grains with different orientations and the Y_2O_3 binder phase, causes significant variations in the modification rate. This is the fundamental reason for the residual grain-boundary step and surface roughness after PAP. Therefore, achieving uniform modification across different grain orientations and phases is essential for obtaining a high-quality surface on AlN ceramics.

Fig. 11 presents the AFM, EBSD (Quantax ED-XS, BRUKER), SEM, and EDX results of the AlN ceramic surface after conventional CMP. Due to grain shed-off occasionally occurs during CMP, and different grain orientations exhibit varying MRR. Consequently, the AFM images reveal an uneven surface, with a resulting surface roughness *Sa* of approximately 10 nm. EDX analysis shows that in the regions marked by black dotted lines, the Al signal was absent while the Y signal was strong, indicating these areas correspond to the Y_2O_3 binder phase. The remaining areas consist of randomly oriented AlN grains with an average grain size of approximately 5 μm. Since the XPS measurement area (ϕ 100 μm) was much larger than the individual grain size, it was challenging to evaluate the modification state of single AlN grains based on XPS alone. To investigate the plasma modification rate across different grain orientations and phases on the surface, plasma irradiation experiments of 30 s, 1 min, and 10 min were performed within the same EBSD-marked region, followed by AFM and EDX characterization. The results are presented in Fig. 12, cross-section C–D was selected to span AlN grains with (110), (001), and (210) orientations, and the relative height variations at different modification stages are summarized in Fig. 12 (d). After 30 s of plasma irradiation, the step height between the (001) and (110) grains decreased by 1.2 nm compared to the surface before irradiation. However, after 1 min of plasma irradiation, the step height returned to its initial value before modification and remained essentially unchanged after 10 min of irradiation. This behavior was attributed to volumetric expansion of the AlN grains induced by the plasma modification process. Upon CF_4 plasma

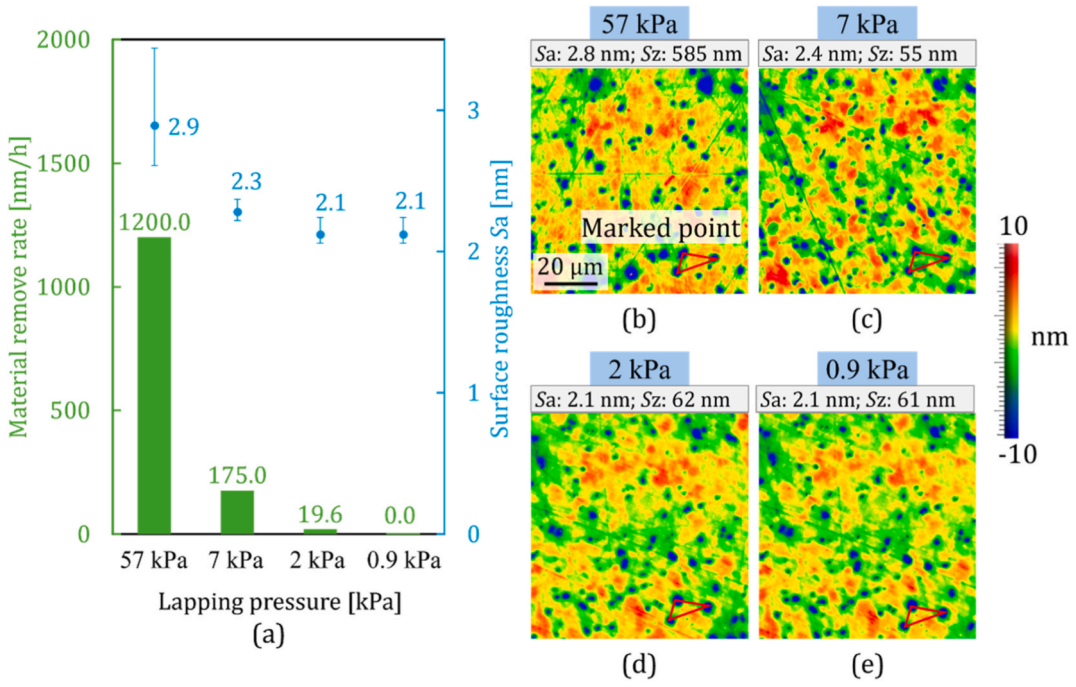

Fig. 6. (a) Material removal rate and surface roughness of the AlN ceramic after lapping under different pressures using #40000 diamond abrasive. SWLI fixed-point observations of the AlN surface after lapping under pressures of (b) 57 kPa, (c) 7 kPa, (d) 2 kPa, and (e) 0.9 kPa.

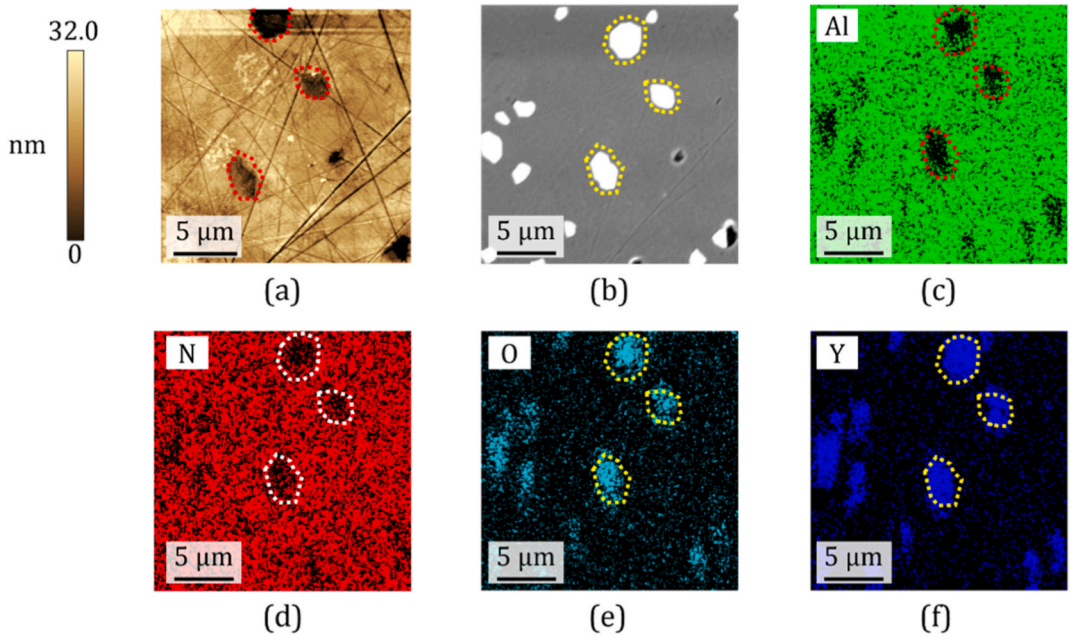

Fig. 7. Surface characterization of the AlN ceramic after lapping under a lapping pressure of 0.9 kPa: (a) AFM image; (b) SEM image; EDX elemental mappings of (c) Al, (d) N, (e) O, and (f) Y.

Table 2
The experimental parameters of plasma irradiation.

Parameters	Conditions
Chamber pressure	37 Pa
Process gas	O_2/CF_4 (Total flow 100 sccm)
Applied RF power	400 W
Plasma irradiation time	30 s/1 min/10 min

irradiation, AlN was converted to AlF_3. Based on the molar masses and densities of AlN and AlF_3, the molar volume increased by approximately 115.1% (theoretical value, without accounting for possible porosity in the AlF_3 modification layer). The initial differences in modification rates among grains with different orientations were reflected in the height variations caused by volumetric expansion. Specifically, the red grains in the EBSD map, corresponding to the (001) polar surface with higher surface chemical activity, exhibit faster modification than the non-polar (110) grains [34,35], resulting in a reduction of step height at the early

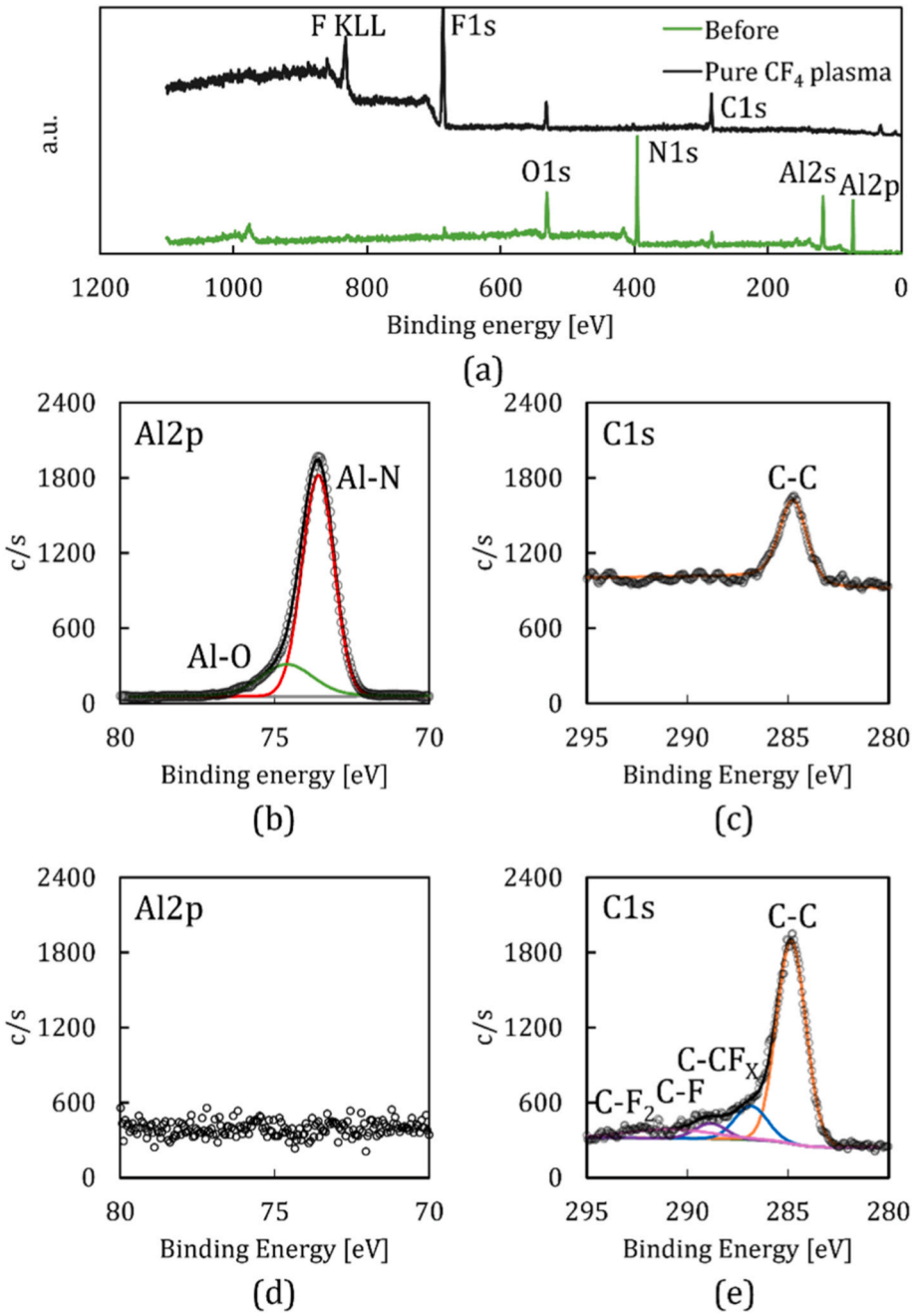

Fig. 8. (a) Full scan spectrum of AlN surface before and after pure CF_4 plasma irradiation for 30 s. XPS spectra of the (b) AlN surface Al2p spectra (c) C1s spectra of AlN before plasma irradiation; (d) Al2p spectra (e) C1s spectra of AlN after pure CF_4 plasma irradiation for 30 s.

stage. As the AlF_3 modification layer thickens, the transport of F radicals through the modified layer to the AlN interface became increasingly limited, significantly reducing the reaction rate at the interface. Consequently, the growth of the modification layer automatically ceased at the maximum depth accessible to F radicals. This depth is independent of the crystallographic orientation of the AlN grains and was primarily determined by the properties of the radicals and the modification layer itself. Therefore, after 1 min of modification, the height differences among the grains have returned to their initial values, indicating that the plasma-induced modification of each grain has self-limited at the same depth, achieving uniform modification across different grain orientations.

In addition, the E–F cross-section containing both AlN grains and the Y_2O_3 binder phase was characterized in the same region. Before irradiation, the Y_2O_3 phase was higher than the adjacent AlN grains. After 30 s of plasma irradiation, the step height decreased by 1.6 nm. However, after 1 min and 10 min of irradiation, the step height returned to its initial value and remained unchanged. This behavior was similar to that observed for AlN grains of different orientations. Due to the relatively large XPS probing area (~100 μm) compared with the typical size of the Y_2O_3 binder phase (~5 μm), the compositional change of the binder phase cannot be directly resolved by XPS measurements. Nevertheless, the EDX analysis (Fig. 12(c)) of the AlN surface after 1 min of plasma modification revealed the presence of F at the locations corresponding to the binder phase, confirming that the Y_2O_3 binder was also modified by F radicals to form YF_3.

Although the initial reaction rates and volumetric expansion of the products differ between AlN and Y_2O_3, as the modification layers of both phases grow and reach the maximum penetration depth of the reactive radicals, plasma-induced modification self-limited, and the height

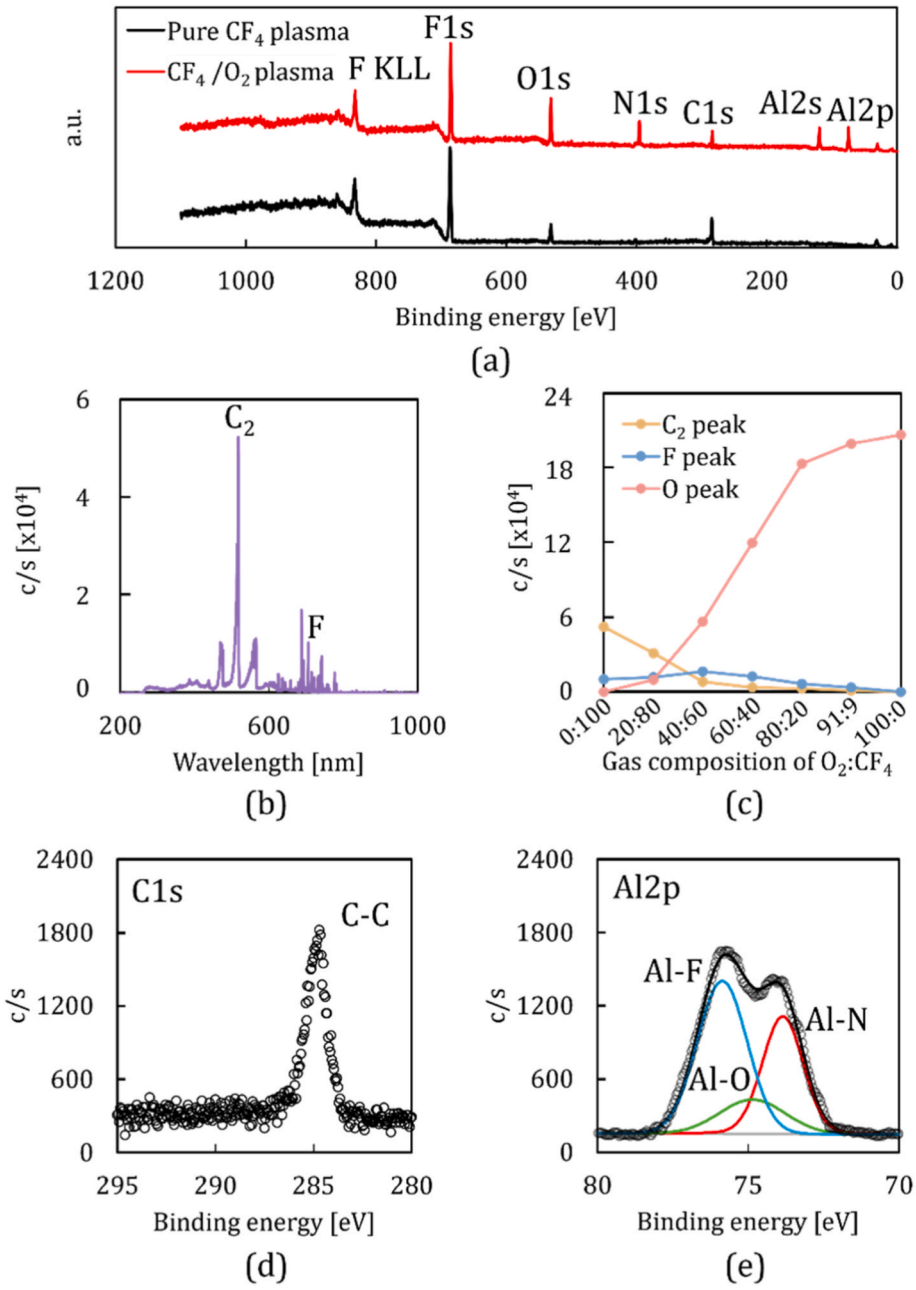

Fig. 9. (a) Full scan spectrum of AlN surface after pure CF_4 plasma irradiation and after O_2/CF_4 flow ratio of 91 sccm/9 sccm for 30 s. (b) OES spectrum of pure CF_4 plasma. (c) Intensities of the C_2, F, and O peaks measured by OES under different O_2/CF_4 ratios. XPS spectra of the AlN surface: (d) C1s and (e) Al2p after plasma irradiation with an O_2/CF_4 flow ratio of 91 sccm/9 sccm for 30 s.

difference returned to its initial value. These observations indicated that self-limiting plasma modification is an effective approach to achieve uniform surface modification on materials with inhomogeneous properties. The EDX analysis (Fig. 12(c)) of AlN surface after 1 min plasma modification further confirmed this conclusion, showing a uniform distribution of F without correlation to the grain or phase distribution.

3.4. High-quality finishing of AlN ceramics by PAP

As shown in Section 3.1, after 1 h of lapping with #40000 diamond grinding stone under a lapping pressure of 0.9 kPa, the surface morphology and roughness of AlN exhibited no significant changes. This result indicated that, at such a low lapping pressure, conventional mechanical lapping neither produced effective material removal nor introduced detectable surface damage on AlN. Therefore, a polishing pressure of 0.9 kPa was initially adopted in the PAP experiments on AlN ceramics. The specific polishing parameters are summarized in Table 3. To verify the removability of the AlF_3 modified layer under the extremely low polishing pressure of 0.9 kPa, XPS spectra were measured on the AlN surface before and after polishing. As shown in Fig. 13(a), the full scan spectra show that F peak was completely removed and the N peak of the original AlN surface reappeared. Specifically, the Al2p and N1s spectra were measured after 1 min of plasma irradiation (Fig. 13(b) and (c)), the AlN surface within the XPS detection depth was fully modified to AlF_3. After 20 s of polishing under a pressure of 0.9 kPa, the surface chemical composition of the AlN substrate is shown in Fig. 13(d). The Al2p spectrum indicated that the Al–F peak disappeared, leaving only the Al–N peak and a weak Al–O peak, consistent with the chemical state of the AlN surface before plasma modification shown in Fig. 10(a). The N1s results further confirmed this observation. These findings

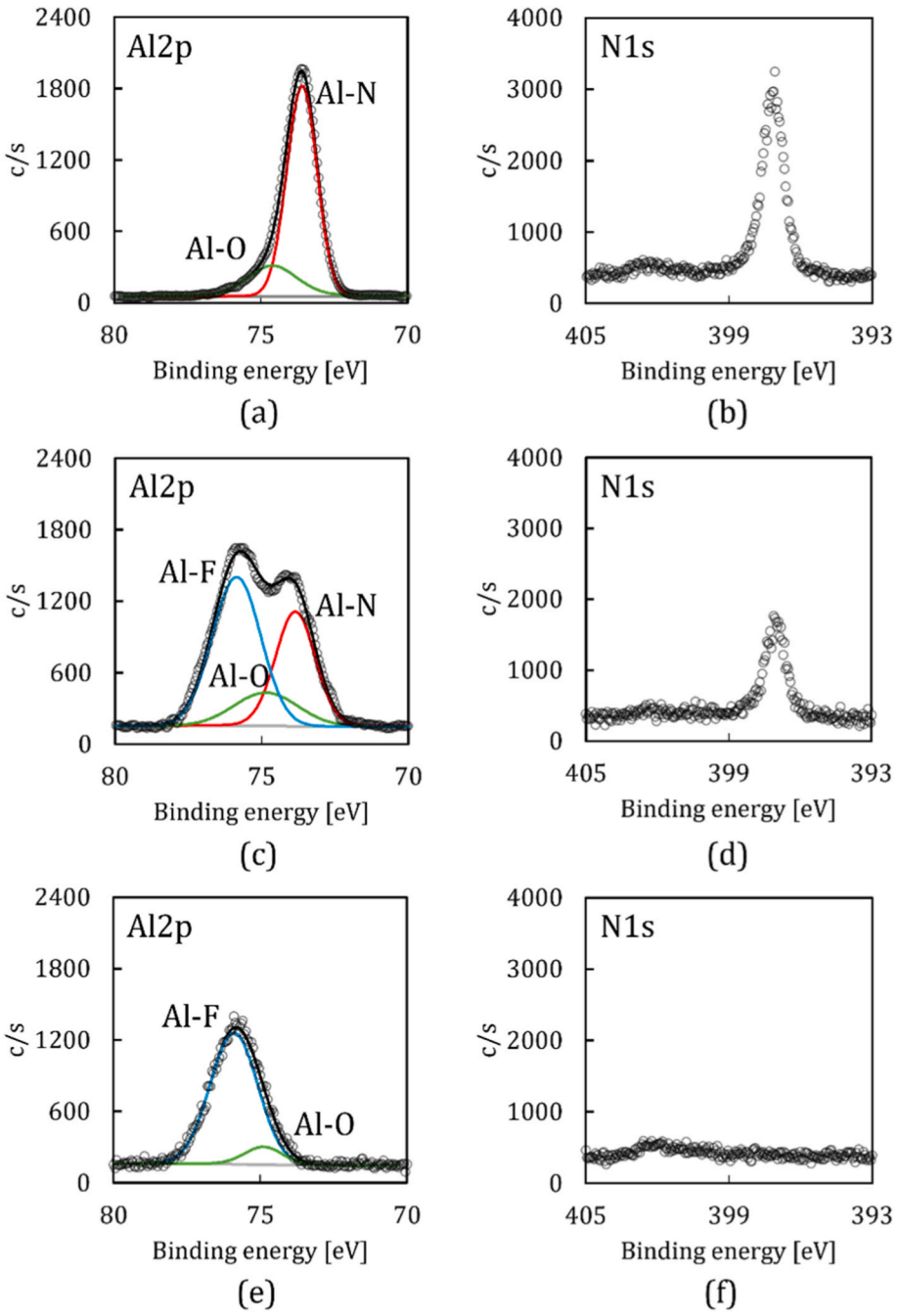

Fig. 10. XPS spectra of the AlN surface (a) Al2p and (b) N1s before plasma irradiation, (c) Al2p and (d) N1s after plasma irradiation for 30 s, (e)Al2p and (f) N1s after plasma irradiation for 1 min.

demonstrated that, even under such an extremely low polishing pressure at which conventional mechanical removal of AlN was ineffective, the AlF_3 modified layer can still be completely removed within a short time, validating the feasibility of selective removal of the surface chemical modification in PAP under ultra-low polishing pressures.

Under the conditions listed in Table 4, AlN substrate that had achieved the lowest surface roughness via the conventional lapping process in Section 3.1 was subjected to 30 cycles of the two-step PAP process, consisting of 1 min of self-limiting plasma modification followed by 20 s of polishing at an ultra-low polishing pressure of 0.9 kPa. The surface morphology after polishing was measured by SWLI. As shown in Fig. 14, the average surface roughness decreased from *Sa* 2.12 nm before PAP to *Sa* 1.26 nm after PAP, while most surface pits were effectively removed. Considering that the reactive plasma can form an AlF_3 modification layer on the AlN surface, which can be easily removed even under ultra-low polishing pressures, the polishing pressure was further reduced to 0.6 kPa. Using the same two-step PAP strategy, 30 additional cycles were performed. As shown in Fig. 14(c), the surface roughness *Sa* was further reduced to 0.86 nm. This improvement is mainly attributed to the further reduction of height differences between different grains and phases. Moreover, since the ultra-low polishing pressure prevents any mechanical damage to the AlN substrate, no scratches were observed on the polished surface.

Furthermore, by measuring the depth of marked scratches on the AlN surface before and after polishing, the material removal depth of the PAP process was quantified. Under conventional lapping at a pressure of 2 kPa, thirty 20-s cycles of purely mechanical removal yielded a total removal depth of only 3.3 nm. At an even lower lapping pressure of 0.9

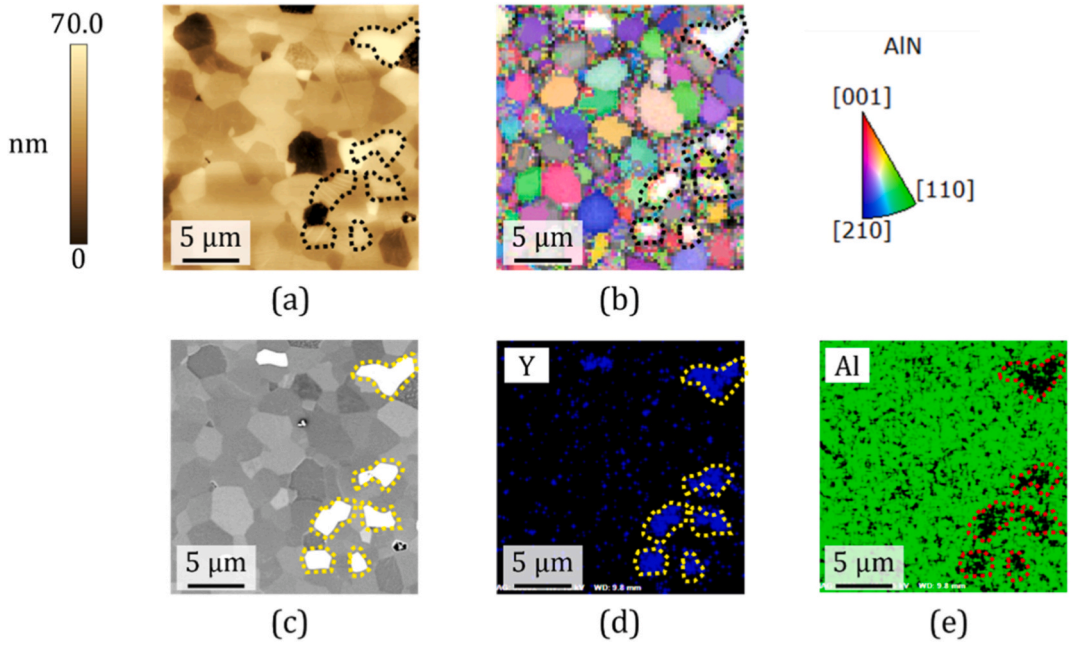

Fig. 11. Surface characterization of the AlN substrate after the CMP process: (a) AFM image, (b) EBSD image, (c) SEM image, and EDX elemental mappings of (d) Y and (e) Al.

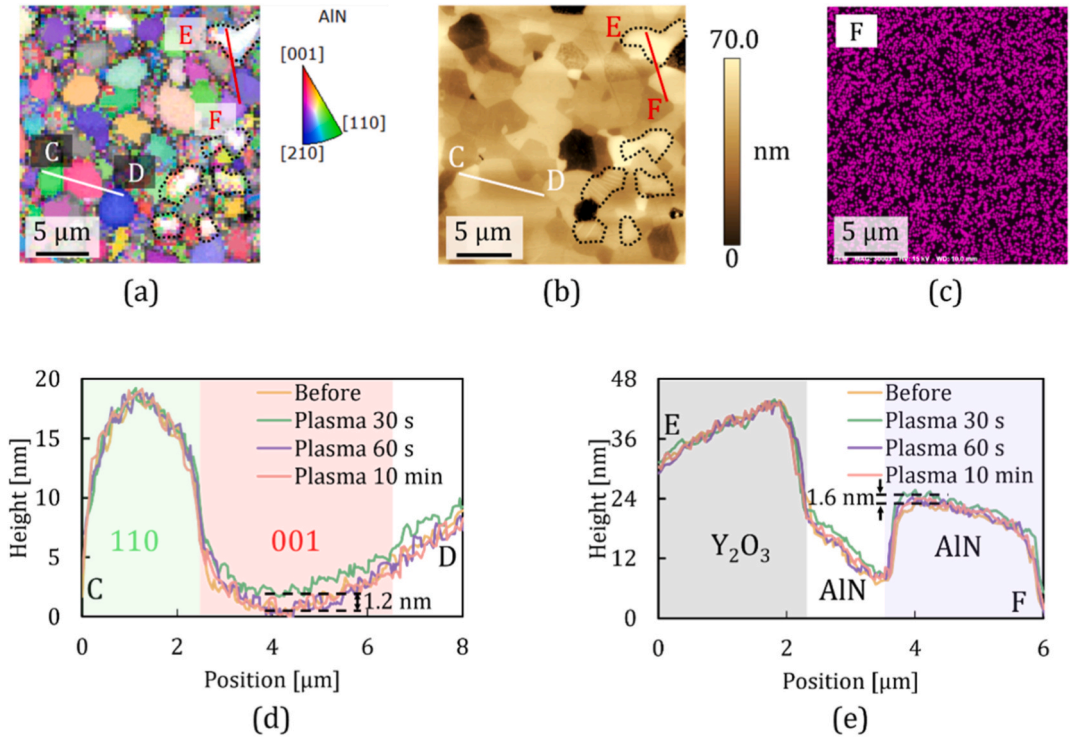

Fig. 12. (a) EBSD image and (b) AFM image of the AlN surface. (c) EDX mapping of the F element after plasma irradiation for 10 min. (d) Cross-section image of AlN grains before and after plasma irradiation for 30 s, 60 s, and 10 min. (e) Cross-section image from the binder material to AlN grains before and after plasma irradiation for 30 s, 60 s, and 10 min.

kPa, virtually no material removal was observed. In contrast, under the two-step PAP process at a polishing pressure of 0.9 kPa, the material removal depth reached 186.7 nm, representing an approximate 59 times increase in efficiency. When the pressure was further reduced to 0.6 kPa, the material removal depth of the two-step PAP remained essentially the same as at 0.9 kPa. This indicated that the overall removal rate in PAP is determined by the plasma modification rate rather than the polishing pressure.

To further evaluate the cross-grain and cross-phase uniformity of PAP, the surface morphology of AlN ceramics before and after PAP was characterized in same region using a laser scanning microscope and AFM (10 × 10 μm area marked by the red box), as shown in Fig. 15. The G–H cross-section was selected, spanning AlN grains with different grain orientations at both ends and the Y_2O_3 binder region in the middle.

Table 3
The experimental parameters of polishing.

Parameters	Conditions
Type of abrasive	Vitrified-bonded diamond (#40000: ϕ 0.125 μm)
Polishing pressure	0.9 kPa
Grinding stone rotation	40 rpm
Substrates rotation	21 rpm
Polishing time	20 s

Fig. 15(a–c) show the AlN surface after purely mechanical lapping before PAP. The step height between AlN grain and Y_2O_3 binder was 23 nm, and the removal depth varied among AlN grains of different orientations, resulting in a grain step of approximately 5 nm. During PAP, the self-limiting nature of the plasma modification enabled uniform modification across different grain orientations and phases. Under ultra-low polishing pressures, the modified layer was sequentially removed from the surface, effectively minimizing the nonuniform material removal caused by variations in

grain orientations and phases observed in conventional mechanical lapping. As a result, the step height between AlN grain and the Y_2O_3 binder at the same location was drastically reduced to 0.8 nm, while the step height among AlN grains of different orientations decreased to 0.5 nm. The surface roughness *Sa* dropped from 3.58 nm to 0.57 nm, demonstrating the exceptional surface smoothing capability of PAP even for polycrystalline and multiphase ceramic materials.

In order to determine whether surface damage is present, the Raman spectroscopy (RAMANtouch, 532 nm, Nanophoton) was employed to evaluate the surface residual stress distribution of the Raman peaks. An ideal stress-free AlN crystal exhibits a characteristic E2 (high) peak at 657.4 cm^{-1}, and the stress magnitude can be calculated from the shift of

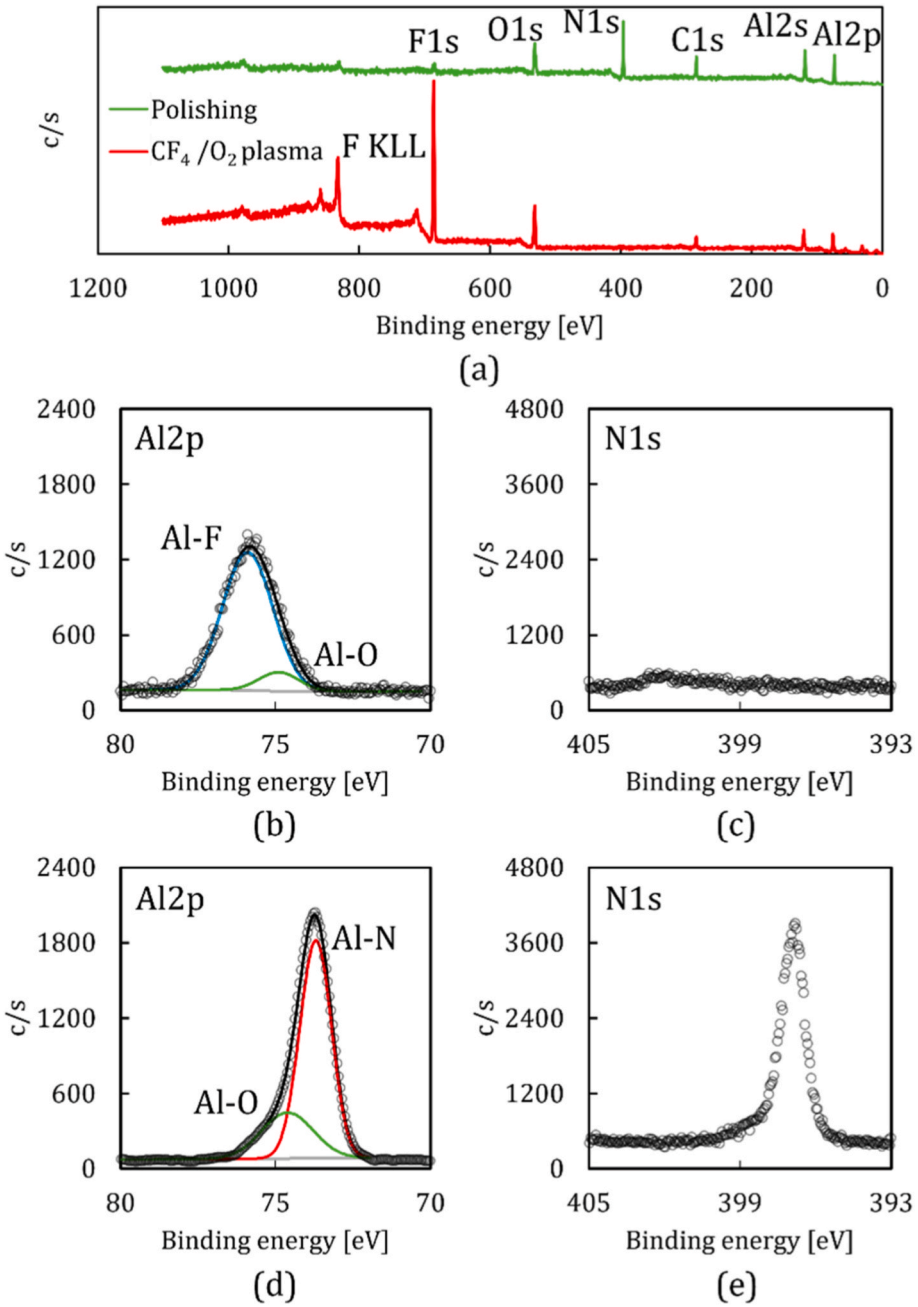

Fig. 13. (a) Full scan spectrum of AlN surface after O_2/CF_4 plasma irradiation for 1 min and after polishing under 0.9 kPa for 20 s. XPS spectra of the AlN surface (b) Al2p and (c) N1s after plasma irradiation for 1 min, (d) Al2p and (e) N1s after polishing under 0.9 kPa for 20 s.

Table 4
The experimental parameters of 2 step plasma assisted polishing.

Parameters	Conditions
Chamber pressure	37 Pa
Process gas	O_2 (91 sccm) CF_4 (9 sccm)
Applied RF power	400 W
Plasma irradiation time	1 min
Type of abrasive	Vitrified-bonded diamond (#40000: ϕ 0.125 μm)
Polishing pressure	0.9 kPa/0.6 kPa
Grinding stone rotation	40 rpm
Substrates rotation	21 rpm
Polishing time	20 s
Number of 2-step PAP circulation	30 times

the 657.4 cm^{-1} peak in the Raman spectrum using a coefficient of 270.3 MPa/cm^{-1} [36]. Fig. 16 shows the residual stress distributions obtained by Raman spectroscopy for the lapped surface, as well as after two-step PAP. As shown in Fig. 16(a), the lapped surface exhibits an overall compressive stress state, which is attributed to sintering-induced residual stress or crystallographic orientation effects in AlN ceramics [36]. In addition, line-shaped stress concentrations were observed, spatially coinciding with the distribution of scratch. In contrast, after 60 times two-step PAP cycles, the scratch-induced surface tensile stress was completely eliminated. These results

indicated that the PAP process, which combines self-limiting plasma modification with selective removal of the modified layer under low polishing pressure, was effective in removing the residual roughness and crystal damage introduced by preceding mechanical processing steps in practical AlN ceramic fabrication. Consequently, the damage-free and ultra-smooth surface can be obtained.

3.5. *Finishing mechanism of plasma self-limiting modification–based ultra-low-pressure polishing*

Fig. 17 illustrates the conceptual schematic of PAP mechanism proposed in this study, centered on the approach of self-limiting plasma modification and ultra-low-pressure selective removal of modified layer. For multiphase ceramics composed of AlN grains with polycrystalline orientations and Y_2O_3 binder phase, conventional mechanical machining relies on increasing the applied pressure to achieve higher MRR. However, this often leads to grain and binder shed-off as well as anisotropic removal, which amplifies pits, steps and consequently degrades the surface roughness. Reducing the applied polishing pressure and using small size abrasives can mitigate the above-mentioned issues. However, when the nominal pressure falls below removal threshold, the abrasives only slide relative to the substrate surface without effectively penetrating the bulk, and material removal cannot be achieved. To enable effective removal under pressures well below this threshold, PAP first modifies the AlN ceramic surface using reactive plasma. As the modified layer grows in thickness, it progressively hinders the transport of radicals, causing the interfacial reaction rate to rapidly decay and reach a saturation thickness within a short time. This phenomenon

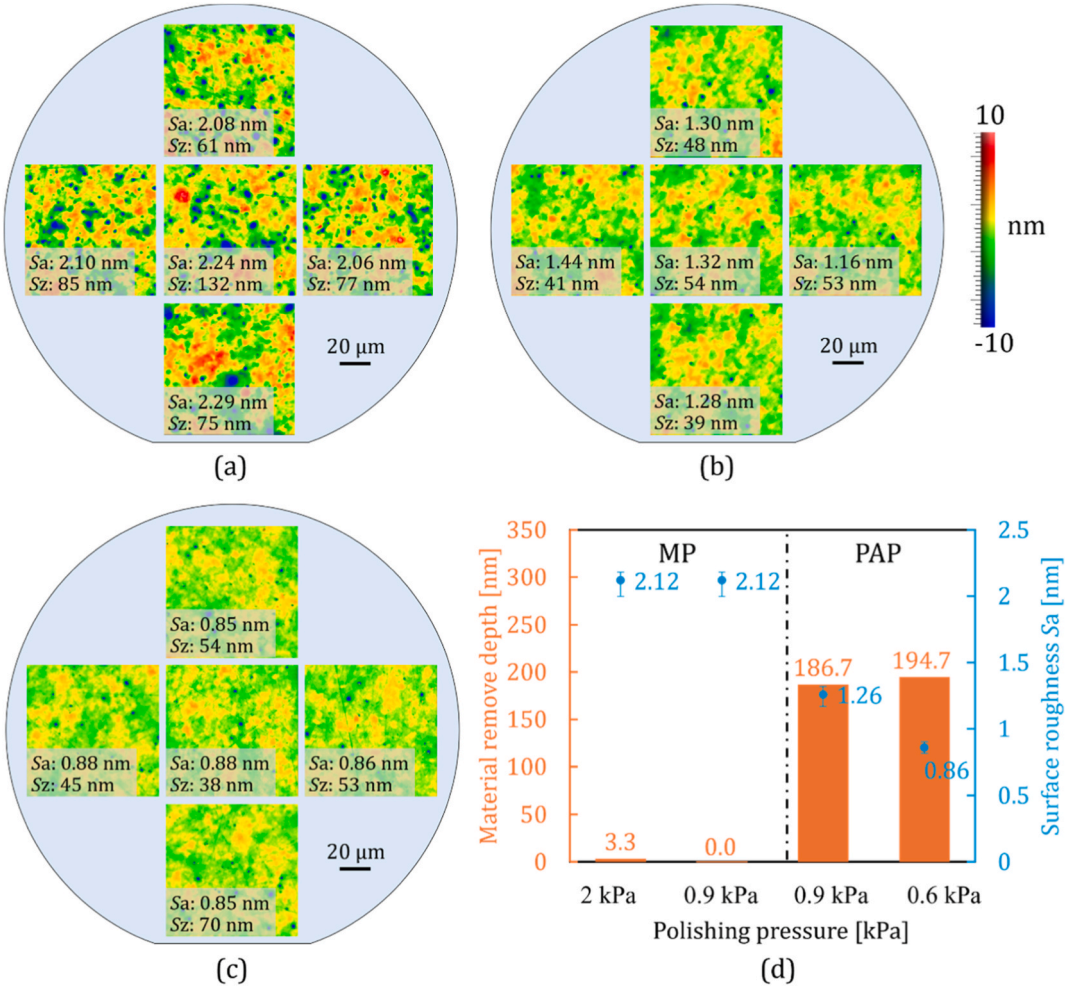

Fig. 14. SWLI images of AlN surface (a) after lapping under pressure of 0.9 kPa, (b) after 2-step PAP under pressure of 0.9 kPa, (c) after 2-step PAP under pressure of 0.6 kPa; (d) Comparison of material removal depth and surface roughness of AlN ceramic after lapping and after PAP under different pressures.

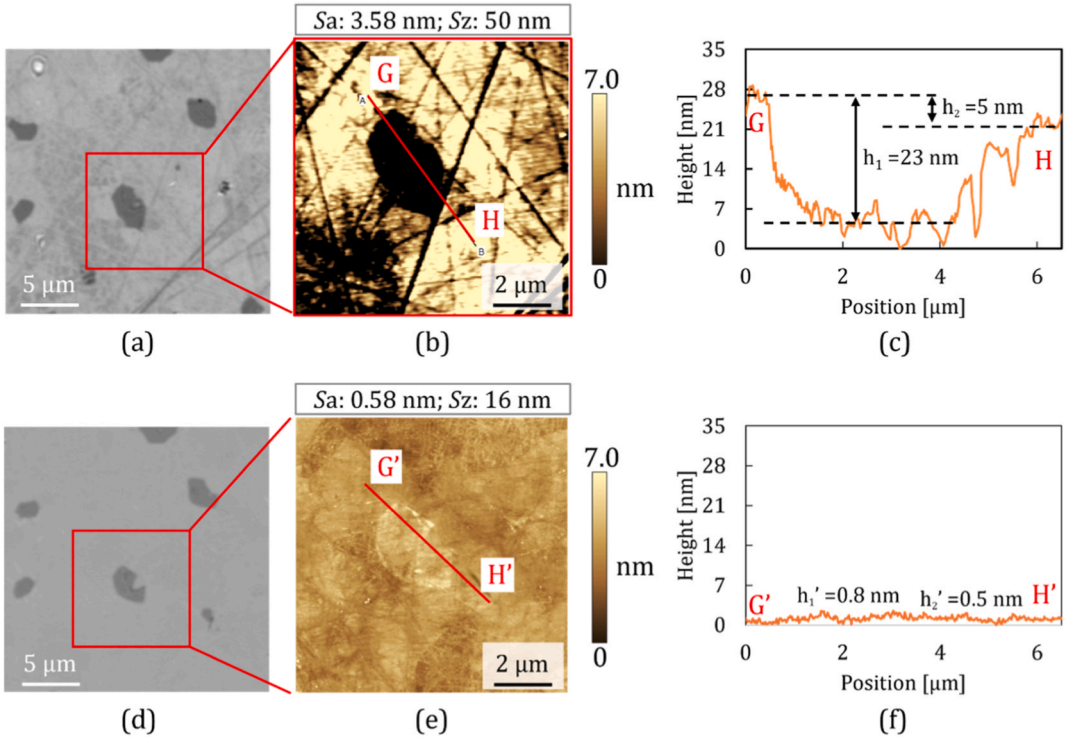

Fig. 15. Surface characterization of the AlN substrate before and after PAP, shown through optical microscope images ((a) before, (d) after), AFM images ((b) before, (e) after), and cross-sectional images from the AlN grain to the binder material ((c) before, (f) after), to illustrate the changes in surface morphology induced by the PAP process.

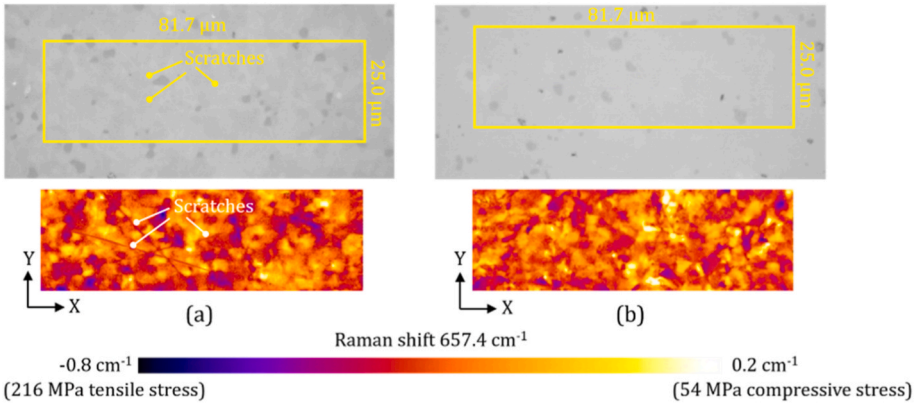

Fig. 16. Optical microscopy images, the residual stress distributions (in yellow rectangle area) on the surfaces of (a) lapped surface, (b) PAP 60 times processed surface measured by confocal Raman microscope with an observation area of 81.7 × 25.0 μm^2 in XY plane.

referred to the self-limiting state. The saturation thickness is primarily determined by the flux and kinetic energy of the radicals as well as the transport properties of the modified layer, and it is relatively insensitive to grain orientation. As a result, a nearly uniform modified layer thickness can be achieved across different grain orientations and phases.

Consequently, the local height variations initially caused by differences in modification rates return to their pre-modification levels once saturation is reached, achieving uniform surface modification. After the surface modification, the polishing stage is conducted under a nominal pressure below the threshold required for effective penetrating of the AlN substrate. This ensures that the unmodified AlN does not experience significant cutting, thereby avoiding brittle fracture and subsurface damage. Meanwhile, the AlF_3 modified layer remains sufficiently susceptible to mechanical removal, allowing its stable and selective removal throughout the polishing process. As a result, a sub-nanometer-level smooth surface of the AlN ceramic was achieved.

At present, CMP remains the primary ultra-precision planarization technique for aluminum nitride ceramics, with other ultra-precision processing methods serving as supplementary approaches. However, existing processes such as CMP, ELID, IBF, and MRF do not exhibit clear advantages in large-scale or batch production, resulting in persistently high processing costs for AlN ceramics. As shown in Table 5, Compared with conventional methods, the two-step PAP process proposed in this study can achieve sub-nanometer surface roughness under ultra-low mechanical pressure while minimizing subsurface damage to the greatest extent. The excellent performance in terms of surface quality, damage suppression, and process stability highlights the practical advantages of this method for ultra-precision finishing of AlN ceramic substrates.

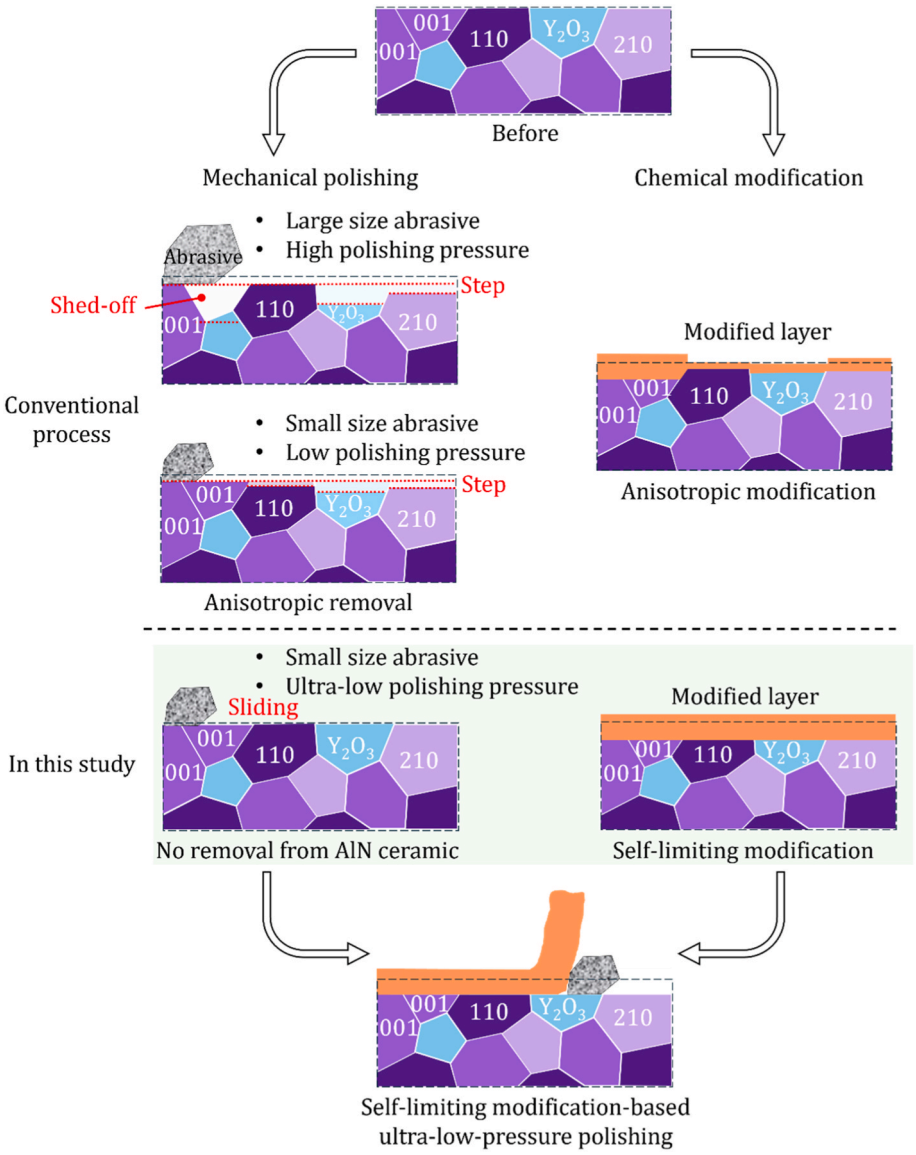

Fig. 17. Schematic diagram of the finishing mechanism in plasma self-limiting modification-based ultra-low-pressure polishing.

Table 5
Comparison of processing methods on AlN ceramics.

Processing method	Best roughness	Processing characteristics	Material removal mechanism
Ultra-precision grinding [37]	*Ra* ≈6 nm	Simple operation, Subsurface damage, Grain-boundary step	Mechanical removal
Chemical mechanical polishing (CMP) [12]	*Ra* ≈6 nm	Damage-free, Grain-boundary step	Non-uniform chemical modification and mechanical removal
Magnetorheological polishing (MRP) [38]	*Ra* ≈22 nm	No tool wear, high cost, Grain-boundary step	Shear force induced by a gradient magnetic field acting on magnetorheological fluid
ELID grinding [11]	*Ra* ≈8 nm	High efficiency, Subsurface damage, Grain-boundary step	Combination of in-process wheel dressing and grinding
Plasma-assisted polishing (conventional) [15]	*Sa* ≈3 nm	Low roughness, Grain-boundary step	Non-uniform plasma modification and removal of the modified layer under low pressure
Plasma-assisted polishing (this study)	*Sa* = 0.8 nm	Sub-nanometer roughness, Damage-free, Grain-boundary step-free	Uniform plasma modification followed by mechanical removal under ultra-low pressure

4. Conclusions

In this study, a two-step PAP process based on plasma self-limiting modification followed by ultra-low-pressure selective removal was developed and its mechanism and effectiveness were systematically validated on AlN ceramics. By optimizing the CF_4/O_2 plasma composition, fluorocarbon deposition on the AlN surface was suppressed, enabling the formation of a self-limiting AlF_3 modification layer, which reached saturation within approximately 1 min with an effective thickness exceeding 7.2 nm. Subsequently, under a polishing pressure below the threshold required for cutting the AlN substrate, small-size fixed diamond abrasives were used to selectively remove the modification layer. Compared with pure mechanical polishing, PAP significantly reduces inter-grain and inter-phase step heights without introducing scratches or subsurface damage. Under a polishing pressure of 0.9 kPa, 30 cycles of 20-s two-step PAP reduced the surface roughness *Sa* of AlN from 2.12 nm to 1.26 nm and further decreased it to 0.86 nm at a polishing pressure of 0.6 kPa. Over the same duration, the material removal depth achieved by two-step PAP was approximately 59 times higher than that of conventional lapping. Multi-technique characterization (AFM, EBSD, SEM, and EDX) confirmed that the modification layer was uniform across different crystal orientations and phases, and that the removal proceeded sequentially from the top-down manner. Pits and grain-boundary steps induced by the Y_2O_3 binder were effectively suppressed. These results demonstrated that the proposed PAP process can achieve sub-nanometer and damage-free finishing of AlN ceramics, with further optimization of the process to achieve higher processing efficiency, it is expected to provide a feasible high-quality surface finishing approach for the industrial fabrication of high-power and high-frequency packaging substrates.

CRediT authorship contribution statement

Tong Tao: Writing – review & editing, Writing – original draft, Validation, Methodology, Investigation, Formal analysis, Data curation, Conceptualization. **Rongyan Sun:** Writing – review & editing, Writing – original draft, Supervision, Resources, Project administration, Methodology, Funding acquisition, Formal analysis, Data curation. **Yuji Ohkubo:** Writing – review & editing. **Kazuya Yamamura:** Writing – review & editing, Supervision, Resources, Funding acquisition.

Declaration of competing interest

The authors declare that they have no known competing financial interests or personal relationships that could have appeared to influence the work reported in this paper.

Acknowledgements

This study was supported by the Japan Society for the Promotion of Science (JSPS) KAKENHI Grant Number 21H05005. We thank CoorsTek, Inc. for providing the AlN substrates, and thank MIZUHO Co., Ltd. for providing the vitrified-bonded grinding stone.

References

[1] T.A. Otitoju, P.U. Okoye, G. Chen, et al., Advanced ceramic components: materials, fabrication, and applications, J. Ind. Eng. Chem. 85 (2020) 34–65.
[2] X. Zhang, L. Ji, L. Zhang, et al., Polishing of alumina ceramic to submicrometer surface roughness by picosecond laser, Surf. Coat. Technol. 397 (2020) 125962.
[3] G.A. Slack, R.A. Tanzilli, R.O. Pohl, et al., The intrinsic thermal conductivity of AlN, J. Phys. Chem. Solid. 48 (1987) 641–647.
[4] R.R. Lee, Development of high thermal conductivity aluminum nitride ceramic, J. Am. Ceram. Soc. 74 (1991) 2242–2249.
[5] Y. Hu, G. Du, N. Chen, A novel approach for Al_2O_3/epoxy composites with high strength and thermal conductivity, Compos. Sci. Technol. 124 (2016) 36–43.
[6] D. Huang, Z. Liu, J. Harris, et al., High thermal conductive AlN substrate for heat dissipation in high-power LEDs, Ceram. Int. 45 (2019) 1412–1415.
[7] M.T. Sarowar, Numerical analysis of a liquid metal cooled mini channel heat sink with five different ceramic substrates, Ceram. Int. 47 (2021) 214–225.
[8] W.M. Yim, R.J. Paff, Thermal expansion of AlN, sapphire, and silicon, J. Appl. Phys. 45 (1974) 1456–1457.
[9] L. Zhao, M. Ke, J. Wang, et al., Insight into mechanism of friction-enhanced chemical behavior in AlN ceramic polishing process, Appl. Surf. Sci. (2025) 164174.
[10] F. Han, W.H. Zhang, W. Gao, et al., Experimental investigation of aluminum nitride ceramics based on compliant finishing process, J. Manuf. Process. 125 (2024) 1–10.
[11] K. Katahira, H. Ohmori, Y. Uehara, et al., ELID grinding characteristics and surface modifying effects of aluminum nitride (AlN) ceramics, Int. J. Mach. Tool Manufact. 45 (2005) 891–896.
[12] Z.Z. Zhou, J.L. Yuan, B.H. Lv, Study on the finishing process for the aluminum nitride substrates, Adv. Mater. Res. 69 (2009) 282–286.
[13] H. Lee, H. Kim, H. Jeong, Approaches to sustainability in chemical mechanical polishing (CMP): a review, Int. J. Precis. Eng. Manuf.–Green Technol. 9 (2022) 349–367.
[14] G. Li, B. Li, Y. Liu, et al., Hydrolysis mechanism of aluminum nitride powder in wet air, Mater. Today Commun. (2025) 113873.
[15] R. Sun, X. Yang, K. Arima, et al., High-quality plasma-assisted polishing of aluminum nitride ceramic, CIRP Ann. 69 (2020) 301–304.
[16] M.A. Moore, A review of two-body abrasive wear, Wear 27 (1974) 1–17.
[17] D.Y. Wi, G.S. Ham, S.H. Kim, et al., Manufacturing and macroscopic properties of Y_2O_3 coating layer on ceramic (AlN) substrate fabricated by aerosol deposition, Arch. Metall. Mater. 63 (2018).
[18] U. Kim, N. Hassan, K. Raju, et al., Flash sintering of AlN ceramics with Y_2O_3 additive, Ceram. Int. 50 (2024) 55042–55054.
[19] Z. Zhang, H. Wu, Z. Zhang, et al., Influence of grain size and grain edge phase on the flexural strength of aluminum nitride ceramics with Y_2O_3 sintering additive, Ceram. Int. 50 (2024) 44957–44964.
[20] G. Hu, C.Q. Chen, K.T. Ramesh, et al., Mechanisms of dynamic deformation and dynamic failure in aluminum nitride, Acta Mater. 60 (2012) 3480–3490.
[21] M.C. Biesinger, Accessing the robustness of adventitious carbon for charge referencing purposes in XPS analysis: insights from a multi-user facility data review, Appl. Surf. Sci. 597 (2022) 153681.
[22] L. Rosenberger, R. Baird, E. McCullen, et al., XPS analysis of aluminum nitride films deposited by plasma source molecular beam epitaxy, Surf. Interface Anal. 40 (2008) 1254–1261.
[23] R. Ramos, G. Cunge, O. Joubert, et al., Plasma/reactor walls interactions in advanced gate etching processes, Thin Solid Films 515 (2007) 4846–4852.
[24] N.H. Chen, C.Y. Wang, J.C. Hwang, et al., MOCVD Al nanocrystals embedded in AlO_XN_Y thin films for nonvolatile memory, ECS J. Solid State Sci. Technol. 1 (2012) P190.
[25] S.N. Hsiao, K. Ishikawa, T. Hayashi, et al., Selective etching of SiN against SiO_2 and poly-Si films in hydrofluoroethane chemistry with $CH_2FCHF_2/O_2/Ar$ mixtures, Appl. Surf. Sci. 541 (2021) 148439.
[26] T. Vandevelde, T.D. Wu, C. Quaeyhaegens, et al., Correlation between the OES plasma composition and the diamond film properties during microwave PA-CVD with nitrogen addition, Thin Solid Films 340 (1999) 159–163.
[27] M.F. Cuddy, E.R. Fisher, Contributions of CF and CF_2 species to fluorocarbon film composition and properties for C_XF_Y PECVD, ACS Appl. Mater. Interfaces 4 (2012) 1733–1741.
[28] V. Kuzmenko, Y. Lebedinskij, A. Miakonkikh, et al., Selective atomic layer etching of Al_2O_3, AlN_X and HfO_2 in conventional ICP etching tools, Vacuum 207 (2023) 111585.
[29] R. Sun, X. Yang, K. Watanabe, et al., Etching characteristics of quartz crystal wafers using argon-based atmospheric-pressure CF_4 plasma stabilized by ethanol addition, Nanomanuf. Metrol. 2 (2019) 168–176.
[30] M.A. Lieberman, A.J. Lichtenberg, Principles of plasma discharges and materials processing, MRS Bull. 30 (1994) 899–901.
[31] D. Hao, Y. Hu, F. Wang, et al., Core–shell structured nAl@F x nanocomposite: preparation and improved combustion performances, J. Energetic Mater. 40 (2022) 61–81.
[32] H. Shinotsuka, S. Tanuma, C.J. Powell, et al., Calculations of electron inelastic mean free paths XII: data for 42 inorganic compounds over 50 eV–200 keV with the full Penn algorithm, Surf. Interface Anal. 51 (2019) 427–457.
[33] J.F. Watts, J. Wolstenholme, An Introduction to Surface Analysis by XPS and AES, Wiley, 2019.
[34] R.M.R. Pinto, V. Gund, C. Calaza, et al., Piezoelectric aluminum nitride thin films: a review of wet and dry etching techniques, Microelectron. Eng. 257 (2022) 111753.
[35] A.P. Shah, A.A. Rahman, A. Bhattacharya, ICP-RIE etching of polar, semi-polar and non-polar AlN: comparison of Cl_2/Ar and $Cl_2/BCl_3/Ar$ plasmas and surface pretreatment, Semicond. Sci. Technol. 30 (2014) 015021.
[36] L. Xie, H. Zhang, X. Xie, et al., Structure and optical properties of AlN crystals grown by metal nitride vapor phase epitaxy with different V/III ratios, ACS Omega 7 (2022) 23497–23502.
[37] H. Li, R. Kang, S. Gao, et al., Surface damage characteristics of AlN ceramics induced by ultra-precision grinding, Mater. Manuf. Process. 37 (2022) 1610–1617.
[38] C. Zheng, B. Chen, X. Yan, et al., The three-point eccentric magnetorheological polishing technology for hard brittle alumina ceramics, Mech. Sci. 13 (2022) 473–483.